Journal of Nuclear Materials 440 (2013) 420–427

Contents lists available at SciVerse ScienceDirect

Journal of Nuclear Materials

journal homepage: www.elsevier.com/locate/jnucmat

High temperature oxidation of fuel cladding candidate materials in steam–hydrogen environments ☆

B.A. Pint *, K.A. Terrani, M.P. Brady, T. Cheng, J.R. Keiser

Oak Ridge National Laboratory, P.O. Box 2008, Oak Ridge, TN 37831-6156, USA

ARTICLE INFO

Article history:
Received 10 January 2013
Accepted 21 May 2013
Available online 1 June 2013

ABSTRACT

Alternative fuel cladding materials to Zr alloys are being investigated for enhanced accident tolerance, which specifically involves oxidation resistance to steam or steam–H_2 environments at ⩾1200 °C for short times. Based on a comparison of a range of commercial and model alloys, conventional austenitic steels do not have sufficient oxidation resistance with only ~18Cr–10Ni. Higher alloyed type 310 stainless steel is protective but Ni is not a desirable alloy addition for this application. Results at 1350 °C indicated that FeCrAl alloys and CVD SiC remain oxidation resistant in steam. At 1200 °C, high (⩾25% Cr) ferritic alloys appear to be good candidates for this application. Higher pressures (up to 20.7 bar) and H_2 additions appeared to have a limited effect on the oxidation behavior of the most oxidation resistant alloys, but higher pressures accelerated the maximum metal loss for less oxidation resistant steels and less metal loss was observed for type 317 L tubing in a H_2–50%H_2O environment at 10.3 bar compared to 100% H_2O.

1. Introduction

To provide larger safety margins and potentially avoid severe core degradation under beyond design basis accident (BDBA) scenarios, one strategy is to develop fuel systems that tolerate severe accident conditions better than the current Zr alloy (e.g. Zircaloy)/UO_2 fuel rods. Under severe accident scenarios in light water reactors (LWRs), e.g. the station blackout events in three units at the Fukushima Daiichi power plant in March 2011 [1], the water level could drop thereby exposing the fuel rods. Under these conditions the drop in heat conductance from the fuel coupled with decay heat production quickly drives the fuel temperature upward. In the case of conventional LWR fuel, the increase in temperature causes the Zr alloy cladding to burst at temperatures between 700 °C and 1100 °C depending on the rod internal pressure [2]. At temperatures above ~1200 °C, self-catalytic enthalpy production due to Zr alloy cladding oxidation (inside by UO_2 but primarily outside by steam) significantly adds to the heat production rate in the core, which quickly surpasses the decay heat production rate in magnitude and results in rapid production of hydrogen as the byproduct of reaction of zirconium with steam. Further accident scenario details will be discussed elsewhere [3]. The purpose of this paper is to consider alternative materials with superior oxidation resistance to Zr cladding alloys such as Zircaloy. A cladding material that could maintain a low oxidation rate for several hours at ⩾1200 °C in steam (⩾2 orders of magnitude lower than Zr alloys) would enhance core safety margins during a BDBA[3].

An example alternative material solution is a ceramic clad fuel using SiC composites [4–6], which could survive much higher temperatures than Zircaloy. While a ceramic cladding has the potential to be protective above 1500 °C, well above the liquidus temperature of ferrous alloys, SiC is difficult to fabricate and has lower ductility than a metallic cladding. Also, the thin SiO_2 layer that forms on SiC is known to be less protective in the presence of water vapor because of the formation of volatile hydroxides [7]. Thus, another strategy is to reexamine stainless steel claddings that were previously used in LWRs, despite the neutronics performance penalty during normal operation compared to Zircaloy [8,9]. To assist in the examination of new alloy compositions, guidelines are needed in order to identify compositions capable of forming protective scales at temperatures of ⩾1200 °C for relatively short (<24 h) periods to simulate severe accident conditions. The goal of this work was to build on initial results [10] and compare the performance of Zircaloy, SiC and various Fe-base alloys in steam and steam–H_2 environments at 800–1350 °C and 1–20 bar. Conventional wrought, oxide dispersion strengthened (ODS) and model alloys were exposed to simulated conditions for 2–48 h in order to determine which classes of alloys are most attractive for further study. Conventional 304-type stainless steel claddings are more oxidation resistant than Zircaloy but do not contain sufficient Cr

☆ Notice: This manuscript has been authored by UT-Battelle, LLC, under Contract No. DE-AC05–00OR22725 with the US Department of Energy. The United States Government retains and the publisher, by accepting the article for publication, acknowledges that the United States Government retains a non-exclusive, paid-up, irrevocable, world-wide license to publish or reproduce the published form of this manuscript, or allow others to do so, for United States Government purposes.

* Corresponding author. Tel.: +1 865 576 2897.
E-mail address: pintba@ornl.gov (B.A. Pint).

0022-3115/$ - see front matter © 2013 Elsevier B.V. All rights reserved.
http://dx.doi.org/10.1016/j.jnucmat.2013.05.047

and Ni levels to be protective at 1200 °C and higher temperatures. The most promising alloys for severe accident tolerance are FeCrAl alloys with ~20 wt.%Cr–5%Al and Fe–Cr alloys with ⩾25%Cr.

2. Experimental procedure

Specimens evaluated in this study included ~12 mm lengths of ~10 mm diameter tubing with 0.65–1.6 mm wall thickness and flat coupons, typically 1–2 mm thick and 4–6 cm^2 in surface area. Compositions are given in Table 1 in mass%. The baseline materials evaluated were tubing sections of Zircaloy-2 (0.9 mm thick wall), Zircaloy-4 (0.8 mm), 304L (1.6 mm), 321 (1 mm), 347L (0.7 mm) and 317L (1 mm). As a baseline comparison for SiC, coupons of Rohm and Haas chemical-vapor-deposited (CVD) SiC were included. Model binary and ternary alloys are referred to by their nominal composition but their actual compositions are given in Table 1 along with the commercial alloys. Oxidation exposures were conducted for 2–48 h in 100% steam and H_2–50%H_2O at temperatures of 800–1350 °C and total pressures up to 20.7 bar (300 psi or 2 MPa). The gas flow rates were constant during exposure but decreased from 95 cm/min at 3.4 bar (50 psi) to 14 cm/min at 20.7 bar at 1200 °C and increased at higher temperatures (111 cm/min at 1350 °C/3.4 bar) and decreased at lower temperatures (67 cm/min at 800 °C/3.4 bar). Multiple specimens were exposed together in the high-pressure tests and were attached to alumina rods (held by a central alumina tube) using Pt wire [11,12]. For 800–1000 °C exposures, an alloy 230 (Ni–22Cr–14W) containment tube was used, which was replaced with a SiC tube for 1200–1350 °C exposures. For thermal gravimetric analysis (TGA) using a Cahn model 1000 microbalance, a quartz tube was used with dry air or 1 bar of Ar–50%H_2O (it was not possible to achieve 100% steam in this TGA system) with an Ar flow rate of 60 cc/min. The TGA produced better kinetic data but was limited to 1200 °C and 1 bar because of the quartz tube. In both the TGA and high-pressure rig, the gas flowed from the bottom to the top of the tube.

Before and after exposure, specimen mass was measured using a Mettler–Toledo model XP205 balance with ±0.01 mg/cm^2 accuracy. After exposure, specimens were metallographically sectioned and examined by light microscopy to determine section loss and oxide thickness and morphology. Metal loss is reported as the average maximum wastage values from three regions of the cross-sections [10]. Additional characterization included electron microprobe analysis (EPMA).

3. Results

3.1. Effect of temperature

Fig. 1 shows mass gain data after 8 h exposures at 800–1350 °C for various alloys in 100% steam. The steam oxidation behavior of Zircaloy has been extensively studied [13–15] and will not be extensively reported here. Mass gains for Zircaloy-2 are shown in Fig. 1 for reference to the more oxidation resistant alloys. The typical 18-8 stainless steels (i.e. types 304L, 321L, 347) all performed similarly in these experiments [12] and the mass change for 304L is shown for reference. The mass change for austenitic alloys can be misleading due to scale spallation. Ferritic alloys have a lower coefficient of thermal expansion difference between metal and thermally-grown oxide; thus, thick oxides are less likely to spall [16]. For example, 304L showed a mass loss at 1000 °C because of scale spallation, Fig. 1. (Recall that the mass gain for an adherent surface oxide is the uptake mass of oxygen while the mass loss for oxide spallation includes the heavier metal cations.) For these alloys, cross-sections are needed to assess the extent of attack [10], as will be shown later. Typical cross-sections of the less protective tubing alloys are shown in Fig. 2. Most were fully consumed or nearly so after only 8 h at 1200 °C. The rates are consistent with a previous study of type 304 stainless steel [17]. In contrast, the most oxidation resistant materials examined over this temperature range were alumina-forming FeCrAl, such as Kanthal alloy APMT® (Advanced Powder Metallurgy Tube), which has some high temperature strength due to its oxide dispersion (Table 1) [18]. This

Table 1
Alloy compositions (mass% or ppmw for S) determined by inductively coupled plasma and combustion techniques.

Alloy	Fe	Zr	Ni	Cr	Al	Mo	Mn	Si	C	O	S	Other
Zircaloy-2	0.14	98.1	0.05	0.10	–	–	–	0.01	0.019	0.115	<	1.42Sn
Zircaloy-4	0.22	98.2	–	0.11	–	–	–	0.01	0.016	0.118	<	1.27Sn
304L	70.3	–	8.27	18.8	0.01	0.27	0.73	0.42	0.028	0.006	<	
317L	64.2	–	11.86	18.9	–	3.13	0.62	0.38	0.023	0.006	10	
321	69.9	–	9.47	17.7	0.03	0.24	1.14	0.45	0.033	0.003	40	
347	68.9	–	9.97	17.5	–	0.16	1.80	0.66	0.040	0.007	150	
310SS	51.9	<	19.5	25.4		0.13	1.89	0.70	0.044	0.006	10	0.15Co, 0.1Cu
AL6XN	48.2		24.1	20.4	0.01	5.98	0.50	0.05	0.012	0.003	<	0.2N, 0.3Cu
Fe20Cr15Ni	65.3	<	15.3	19.4	<	<	<	0.01	0.002	0.043	47	
Fe20Cr20Ni	60.1	<	20.1	19.7	<	<	<	0.01	0.001	0.042	41	
Fe20Cr20Ni+	57.9	<	19.9	20.2	0.03	<	1.61	0.22	0.001	0.003	<	0.12La
Fe20Cr25Ni	55.4	<	24.8	19.5	<	<	<	<	0.002	0.043	45	
HR120	35.0	<	37.6	24.7	0.09	0.28	0.73	0.24	0.059	0.003	<	0.61Nb, 0.2Cu
P91	88.7	<	0.16	8.75	0.03	0.98	0.46	0.28	0.102	0.004	30	0.46Nb, 0.24V
Fe–15Cr	85.1	–	<	14.8	<	<	<	<	0.003	0.004	20	
Fe–20Cr	80.3	–	<	19.7	<	<	<	0.01	0.002	0.003	15	
Fe–25Cr	74.6	–	–	25.3	–	–	–	0.02	0.004	0.037	10	
ODM401	83.9	0.001	0.13	14.0	0.06	0.30	0.04	0.04	0.013	0.191	52	0.21Y, 1.0Ti
E–Brite	72.6		0.13	25.8		1.00	<	0.22	0.003	0.003	100	0.1Nb, 0.1V
AL294C	66.1		0.19	28.6	0.07	3.70	0.21	0.27	0.017	0.002	<	0.3Nb, 0.37Ti
PM2000	74.6	–	0.1	18.9	5.1	0.01	0.11	0.04	0.01	0.25	8	0.37Y, 0.45Ti
APMT	69.0	0.10	0.12	21.6	4.9	2.8	0.10	0.53	0.030	0.049	<	0.12Y, 0.16Hf
Ohmaloy30	82.8	<	0.58	12.6	2.6	0.05	0.41	0.26	0.017	<	<3	0.34Ti, 0.1V
Ohmaloy40	81.7	<	0.53	12.7	3.6	0.10	0.37	0.22	0.021	<	<3	0.34Ti, 0.13V
NITE-SiC	0.32	–	0.04	0.09	0.38	–	–	67.8	27.7	2.94	<	0.44Y
CVD-SiC	–	–	0.01	–	–	–	–	69.8	30.2	0.003	<	–

Note: < denotes below the detectable limit of 0.01% or 0.001% for interstitials.

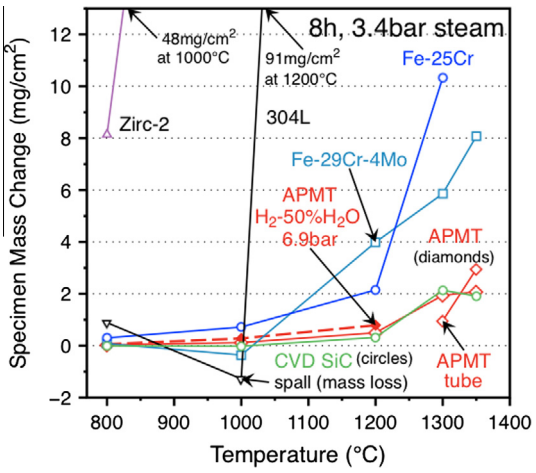

Fig. 1. Specimen mass change data after 8 h exposures in 3.4 bar steam as a function of temperature. Additional data is included for 6.9 bar H_2–50%H_2O for APMT (dashed line).

material showed a low mass gain even at 1350 °C due to the formation of a protective, external alumina scale, which is less affected by H_2O than SiO_2 or Cr_2O_3 [7]. As a representative of the various SiC composites, CVD SiC also showed low mass changes from 800 to 1350 °C, Fig. 1. Another class of alloys of interest is ferritic steels and results for two alloys are shown in Fig. 1, a model binary Fe–25Cr alloy and a commercial (Allegheny Ludlum) alloy AL294C, Table 1. Both alloys showed increased attack above 1200 °C. The most oxidation resistant materials began to strongly differentiate at 1200 °C so more attention was focused on the highest temperature conditions and less devoted to the experimental results at 800 °C and 1000 °C where thinner reaction products were formed and less differentiation occurred among the various alloys, Fig. 1.

Fig. 3 shows example cross-sections of the oxides formed on APMT and CVD SiC at the highest temperatures investigated in this study at 3.4 bar steam. Fig. 3a shows the protective external alumina scale formed on APMT after 48 h at 1200 °C. Fig. 3b and c show APMT after 8 h at 1300 °C and 1350 °C, respectively. In each case, the alumina forms a solid-state diffusion barrier that limits the oxidation rate to ionic diffusion (mainly anions) through this oxide layer, which is relatively inert to the presence of steam. The reactive element (RE) additions of Y and Hf in this alloy are essential to the good scale adhesion observed [19,20]. No internal oxidation was observed at these temperatures, Fig. 3a–c. The RE additions in APMT are tied up as oxides in the alloy and are not available to form oxide stringers. The thin SiO_2 layer formed on CVD SiC at 1350 °C is shown in Fig. 3d. The layer thickness is affected by the gas velocity, which affects the $Si(OH)_4$ volatilization [21].

3.2. Reaction kinetics at 1200 °C

To determine the reaction rates at 1200 °C, a time series of specimens was performed in 3.4 bar steam, Fig. 4a. The mass change data are plotted versus the square root of time to reflect the parabolic reaction rate expected for these materials [22]. As mentioned previously, due to scale spallation, the mass change data are not appropriate for determining reaction rates, especially for the austenitic type 310 stainless steel which exhibited much lower mass gains than expected. The ferritic alloys AL294C and E-Brite both showed rate constants of $2–4 \times 10^{-10}$ g^2/cm^4 s consistent with chromia scale formation at 1200 °C, but without the CrO_3 volatilization loss found when O_2 reacts with Cr_2O_3 [23]. For the slower growing alumina scale on APMT, the rate constant was 100 times lower than for chromia scales. The rates for alumina are similar to those observed in air or O_2 [19,20].

More accurate reaction rates were determined by TGA, Fig. 4b. As expected, the rates were similar in both conditions for APMT because this alloy showed no scale spallation. However, the 310SS mass gain was much higher in the TGA experiment, comparable to the ferritic alloys in Fig. 4a. (The O_2 partial pressure is too low in these experiments to form sufficient volatile $CrO_2(OH)_2$ even with the difference in total steam pressure [24].) Upon cooling in the TGA, the 310SS specimen spalled resulting in a mass loss. Likewise, the ferritic alloys showed slightly higher rates in the TGA

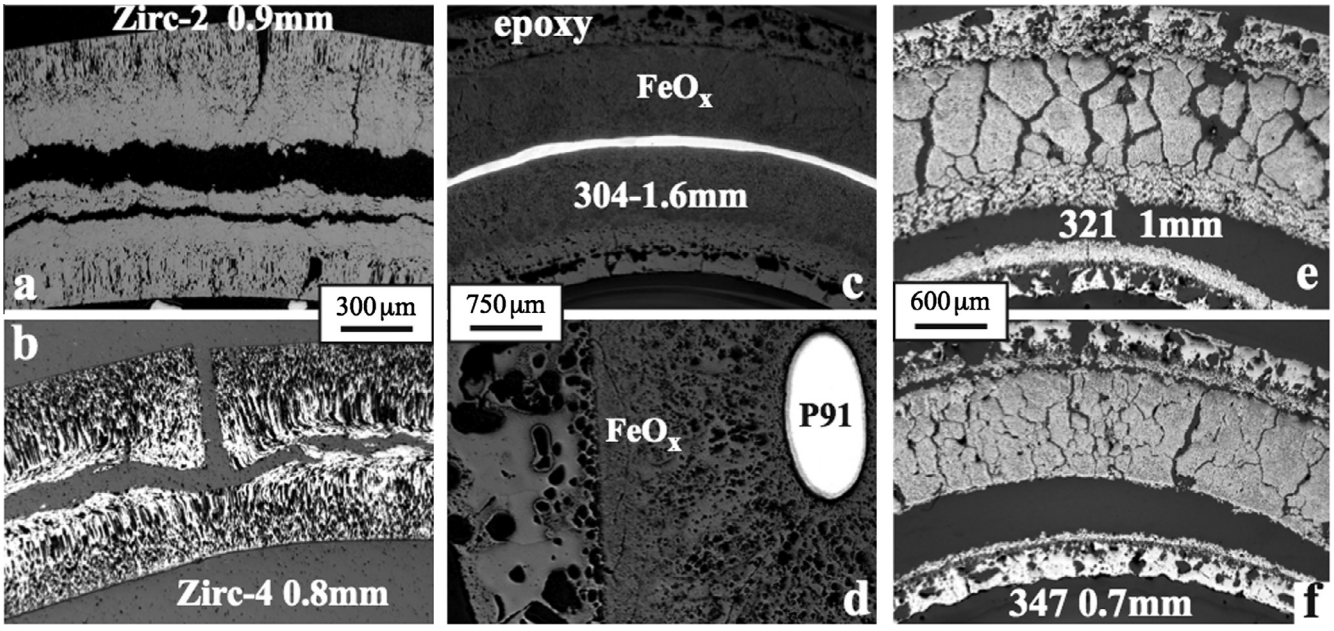

Fig. 2. Example cross-sections of the less oxidation resistant tubing alloys exposed for 8 h at 1200 °C in 10.3 bar (150 psi) including (a) Zircaloy 2, (b) Zircaloy 4, (c) type 304, (d) P91, (e) type 321 and (f) type 347 stainless steel. The initial tubing wall thickness is noted.

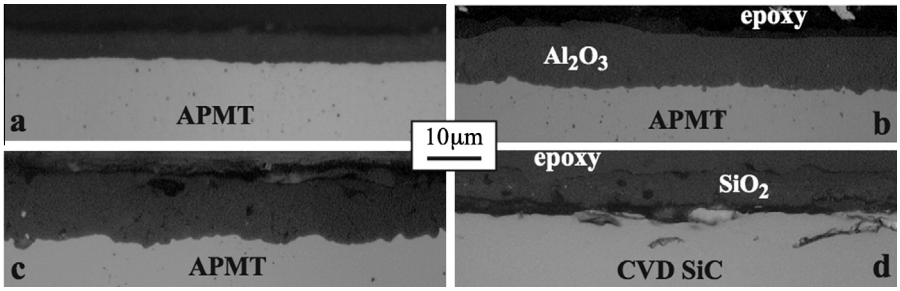

Fig. 3. Light microscopy of polished cross-sections of APMT after (a) 48 h at 1200 °C, (b) 8 h at 1300 °C (c) 8 h at 1350 °C and (d) CVD SiC after 8 h at 1350 °C.

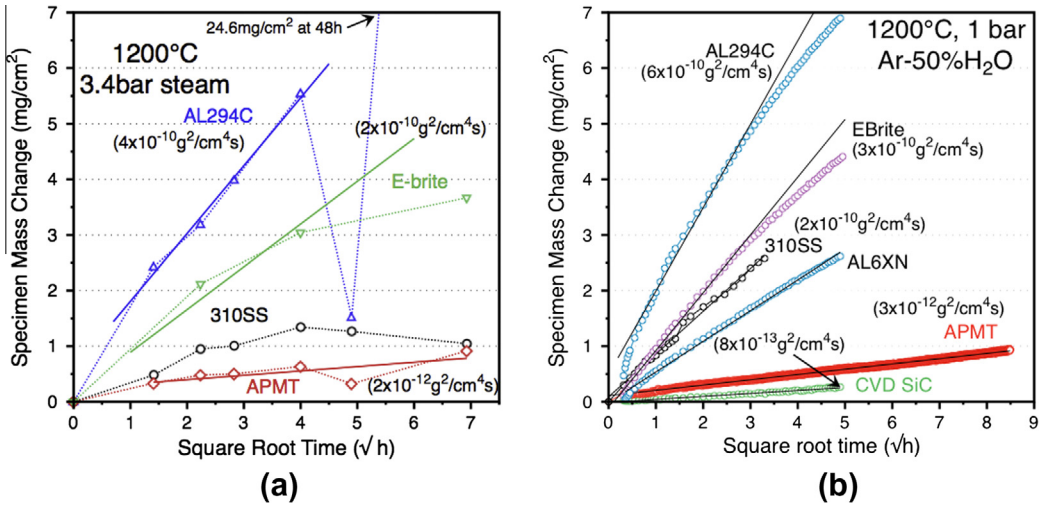

Fig. 4. Specimen mass change data for a series of specimens exposed at different times in (a) isothermal exposures in 3.4 bar steam at 1200 °C and (b) thermal gravimetric mass gain data at 1200 °C in 1 bar Ar–50%H_2O.

experiment due to some degree of spallation in the high-pressure experiments, e.g. the rate for AL294C increased from 4×10^{-10} to 6×10^{-10} g^2/cm^4 s in the TGA, Fig. 4. A low mass gain also was observed for the CVD SiC specimen in the TGA experiment, Fig. 4b.

Fig. 5a summarizes some of the rate constants measured at 1000–1200 °C in an Arrhenius plot assuming parabolic kinetics in all cases. As expected, the rate on type 310 stainless steel was highest followed by the alumina-forming FeCrAl alloy APMT. The slowest rates were measured for CVD SiC. To illustrate the effect of steam on the reaction rates, exposures also were made in dry air. The rates for 310SS and CVD SiC were both lower in dry air indicating a detrimental effect of steam on the oxidation rate. In contrast, the reaction rates for APMT were very similar in air and steam at 1200 °C. However, at 1000 °C, the rate in air was much lower than the equivalent rate observed in steam. This difference is attributed to water vapor stabilizing metastable cubic alumina

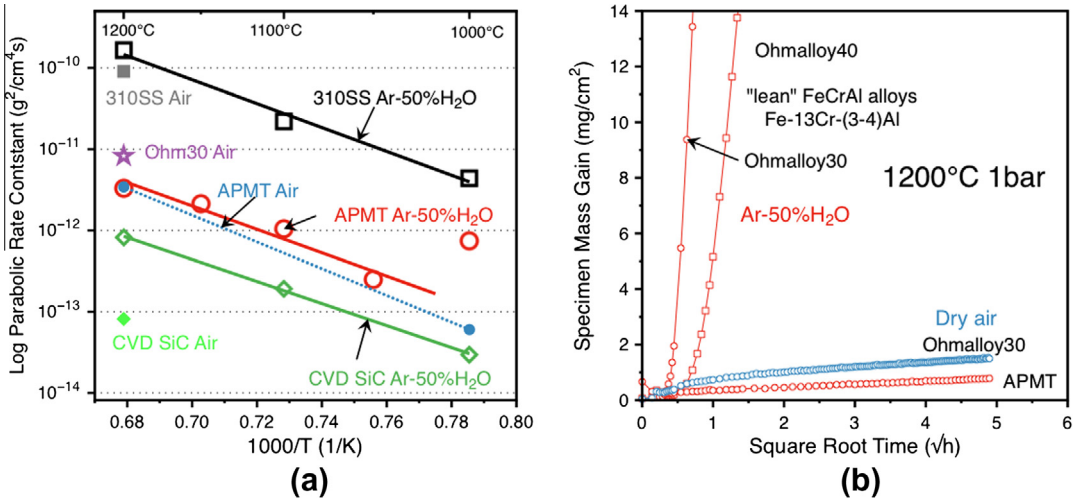

Fig. 5. (a) Arrhenius plot of the parabolic reaction rates for several materials and (b) comparison of mass gain for FeCrAl alloys at 1200 °C in Ar–50%H_2O and dry air.

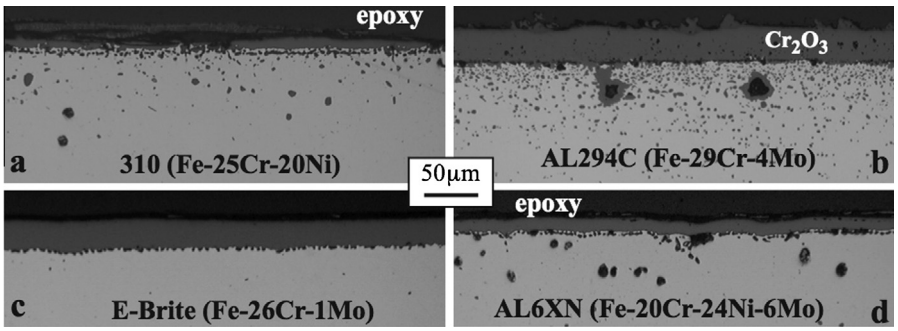

Fig. 6. Light microscopy of polished cross-sections after 48 h at 1200 °C in 3.4 bar steam (a) 310SS, (b) Fe–29Cr–4Mo (c) E-Brite and (d) Fe–25Cr.

phases such as θ-Al_2O_3 [25], which is known to grow much faster than the stable α-Al_2O_3 phase [26]. Other studies of the same or similar alloys have not observed this effect of water vapor [27,28]. However, those studies were performed in wet oxygen rather than wet Ar.

In addition to APMT, "lean" FeCrAl alloys with only 13Cr (Table 1) also were studied and these alloys showed breakaway oxidation at 1200 °C in Ar–H_2O, indicating that a protective alumina scale could not be formed under these conditions, Fig. 5b. However, in dry air a protective oxide was formed. The slightly higher rate constant for Ohmaloy 30 compared to APMT likely reflects the lack of a RE addition in the former, Fig. 5a. The Y and Hf in APMT are well known to reduce the rate constant at 1200 °C by a factor of 2–3 [19,20].

For the TGA work on chromia-forming alloys, 310SS was studied extensively but several more alloys were included at 1200 °C, with some variation in the reaction rates, Fig. 4b. In order to confirm that a similar ordering was observed in the higher pressure experiments, Fig. 6 compares the chromia scale thicknesses of several alloys after 48 h exposures at 1200 °C in 3.4 bar steam. There was obvious scale spallation in some locations for the 310SS specimen, Fig. 6a. Based on the mass change, the ferritic alloys formed more adherent oxides. However, the cross-sections revealed significantly more internal oxidation was observed for the AL294C specimen (Fig. 6b), likely due to the presence of 0.4%Ti, 0.3%Si and 0.3%Nb in this alloy compared to E-Brite (0.2%Si and 0.1%Nb), which exhibited very little internal oxidation, Fig. 6c. In this case, only a darker discontinuous phase at the chromia-metal interface was observed, which was identified as SiO_2 by EPMA. Because silica is more thermodynamically stable than chromia, it can form beneath the chromia layer where the oxygen partial pressure is equal to the Cr/Cr_2O_3 equilibrium [29]. The scale thickness on E-Brite was very similar to the binary model Fe–25Cr alloy (not shown) that contained only 0.02%Si and did not show any indication of SiO_2 formation [10]. The similar scale thickness suggests that an inner silica layer is not truly protective in these conditions. Finally, Fig. 6d shows the thinner scale formed on AL6XN, similar to the thinner scale formed on type 310 stainless steel. Both austenitic steels formed a thinner chromia layer than the ferritic steel but the scale appeared to be more adherent on AL6XN than on 310SS.

3.3. Alloy composition effects

A wider range of model alloys was exposed at a few conditions in order to assess which composition ranges were most resistant to these environments. Fig. 7 summarizes a wide range of observations as a function of Cr content, mainly in 3.4 bar steam and for alloys where spallation was not significant. For the model Fe–Cr alloys, Fig. 7a shows that 25%Cr was needed to form a protective Cr_2O_3 scale at 1200 °C. Fig. 7b shows that Fe–15Cr was protective at 800 °C but not at higher temperatures and Fe–20Cr showed higher mass gain at 1200 °C indicating the onset of breakaway oxidation. Both the model and commercial alloys with higher Cr contents showed protective behavior at 1200 °C. Fig. 8a shows the onset of breakaway oxidation for Fe–20Cr with large FeO_x nodules forming after only 2 h at 1200 °C in 3.4 bar steam. However, in other areas, a protective chromia scale formed, Fig. 8b. Much larger

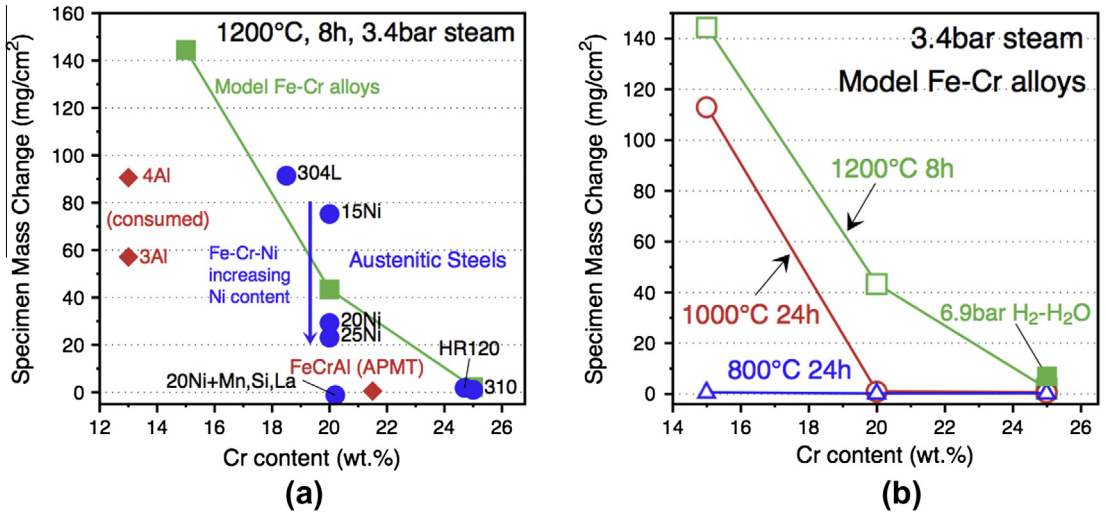

Fig. 7. Specimen mass change as a function of Cr content (a) after 8 h at 1200 °C in 3.4 bar steam and (b) Fe–Cr model alloys at 800–1200 °C.

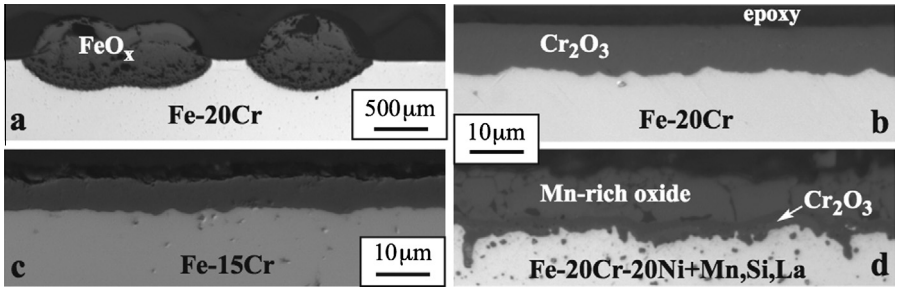

Fig. 8. Light microscopy of polished cross-sections after exposure for 2 h at 1200 °C in 3.4 bar steam (a) and (b) Fe–20Cr, (c) Fe–15Cr and (d) Fe–20Cr–20Ni + Mn,Si,La.

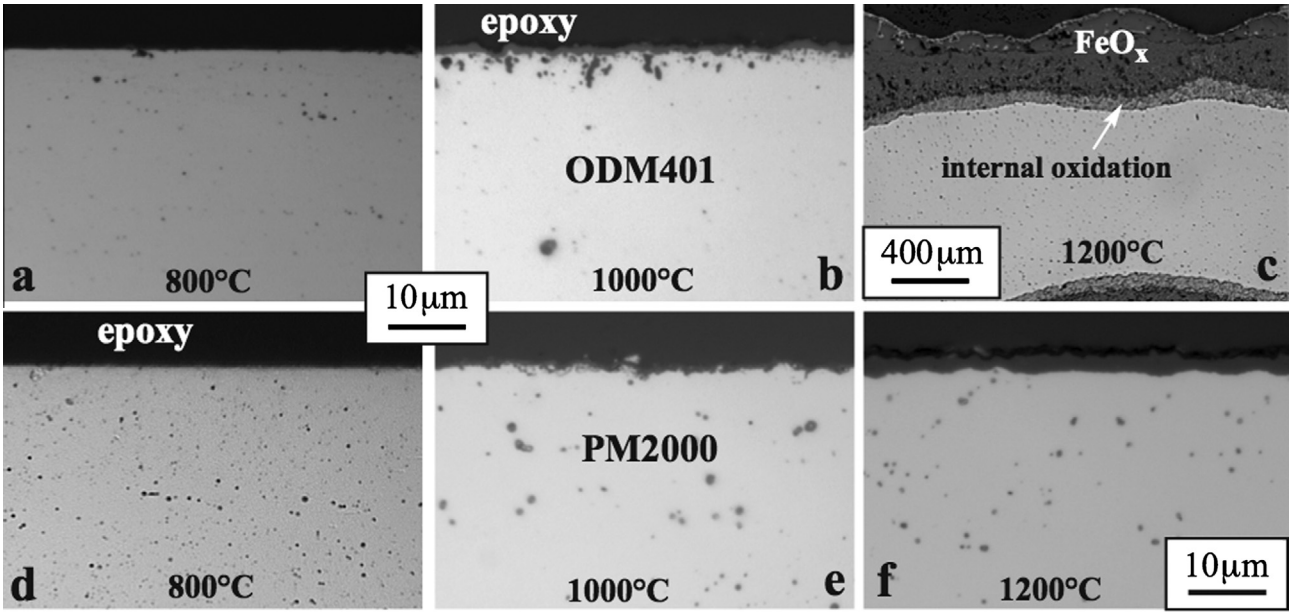

Fig. 9. Light microscopy of polished cross-sections after exposure for 8 h in H_2–50%H_2O at 10.3 bar at (a and d) 800 °C, (b and e) 1000 °C and (c and f) 1200 °C for (a–c) alloy ODM401 (ODS Fe–14Cr) and (d–f) alloy PM2000 (ODS FeCrAl).

FeO_x nodules formed on Fe–15Cr under these conditions as suggested by the higher mass gain in Fig. 7b; however, a few areas could be found where a thin chromia scale formed, Fig. 8c. There was not sufficient Cr in these alloys to retain protective scale formation. Even Fe–25Cr formed thick FeO_x nodules in some locations after 48 h at 1200 °C and at higher temperatures, as suggested by the high mass gains in Fig. 1.

Returning to Fig. 7a, a series of model ternary Fe–20Cr–Ni alloys illustrated the benefit of higher Ni contents on oxidation resistance. Other elements besides Ni can improve the oxidation resistance of austenitic steels, especially Mn, Si and RE additions like La [30,31]. These elements result in a more complex reaction product as was shown previously with the SiO_2 inner layer. Along with Si and La, the addition of Mn reduced the mass gain and suppressed the formation of FeO_x on Fe–20Cr–20Ni, Fig. 7a. Fig. 8d shows that a thick Mn-rich outer oxide formed (identified by EPMA). Whether the formation of this Mn-rich oxide or a synergistic increase in Cr transport (as is found with Si [32]) explains the benefit has not been determined.

Fig. 7a also shows the poor results for leaner FeCrAl compositions with 13Cr and 3–4%Al alloys, as was shown at 1 bar Ar–50%H_2O in Fig. 5b. These alloys are of interest because they are easier to fabricate and join than typical Fe–20Cr–5Al alloys and reflect the potential result of simply adding Al to current Fe–(9–14)Cr ODS alloys [33]. Fig. 9 illustrates the benefit of Al in ODS alloys (only included in a few experiments because of limited availability). The Fe–14Cr ODM401 [34] formed a protective Cr-rich oxide at 800 °C and 1000 °C in 10.3 bar of H_2–50%H_2O but not at 1200 °C, Fig. 9a–c. In contrast, ODS FeCrAl (PM2000) formed a thin protective Al-rich oxide at all three conditions, Fig. 9d–f, very similar to APMT.

3.4. Effect of pressure and hydrogen

Several experiments were conducted to evaluate the effect of total pressure and H_2 in the environment. For the most oxidation-resistant materials, there appeared to be little change with higher pressure and the addition of H_2. For example, the dashed line in Fig. 1 shows the minor effect of higher total pressure with the addition of H_2. Likewise, Fig. 7b shows only a slight change in the mass gain for Fe–25Cr for the 6.9 bar H_2–50%H_2O environment. A more substantial effect of pressure was observed for the lower alloyed steels. Fig. 10 shows maximum metal loss results for the 317L tubing as a function of temperature and as a function of time at 1200 °C. (A few of these data were reported previously [10].) For this material that could not form a protective scale (based on the high mass gains), the increased steam partial pressure appeared to accelerate the rate of metal loss at 1200 °C. This effect is further illustrated in cross-sections in Fig. 11 showing some of the images that were used to generate the metal loss data

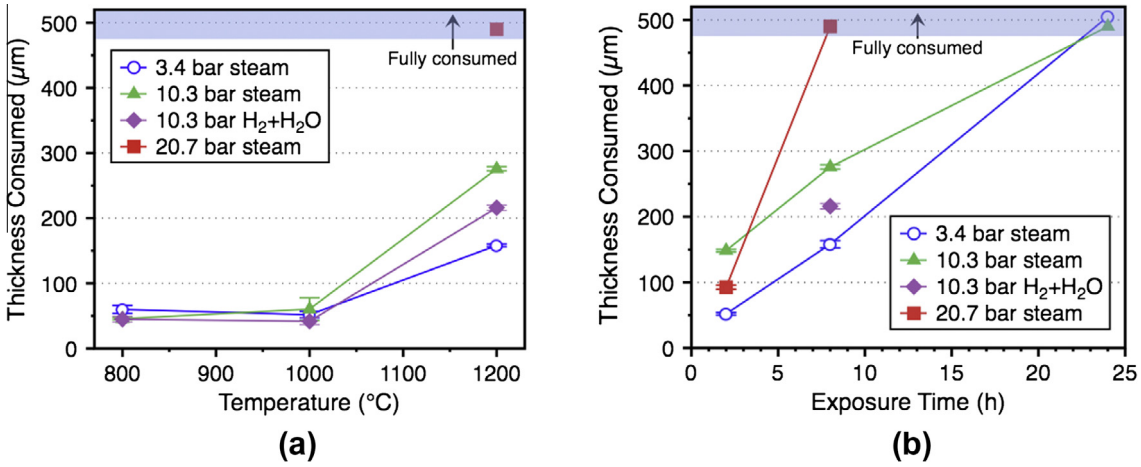

Fig. 10. Metal loss for type 317L tubing in several pressures and two environments (a) as a function of temperature for 8 h exposures and (b) as a function of time at 1200 °C.

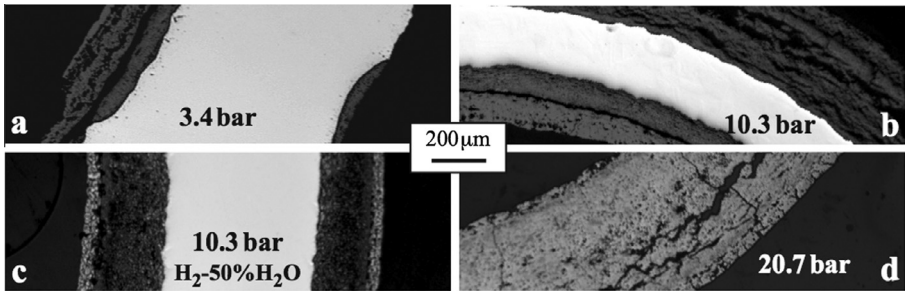

Fig. 11. Light microscopy of polished cross-sections of 317L tubing after 8 h at 1200 °C (a) 3.4 bar steam, (b) 6.9 bar steam, (c) 6.9 bar H_2–50%H_2O and (d) 20.7 bar steam.

in Fig. 10. (317L performed better than the other stainless steels tubes that were fully consumed after a similar exposure, Fig. 2.) The laminate-structured scales observed are typical of steels that rapidly oxidize in steam [35]. At 10.3 bar (150psi), switching from 100% H_2O to H_2–50%H_2O decreased the maximum metal loss, Fig. 10. This difference can be seen in the cross-sections in Fig. 11b and c and suggests that H_2–H_2O environments are less aggressive than steam alone. From these results, it appears that the reaction rate is dominated by the steam partial pressure without any significant effect of the presence of H_2.

4. Discussion and future work

A large number of experiments were conducted as part of this initial study [12] with specific data reported to support the most important findings. As noted previously, the results were focused on the $\geqslant$1200 °C experiments because there was less differentiation in performance at lower temperatures. Fig. 9 provides an example that the thin oxides formed at lower temperatures were also difficult to image, without higher resolution characterization techniques. For severe accident scenarios, there is greater interest in higher temperatures and in determining the maximum temperature that candidate materials remain protective.

There is a tendency in screening studies such as this one to simply test a large number of commercial alloys. The importance of the model Fe–Cr alloys is to establish how much Cr would be needed for protective behavior, as illustrated in Fig. 7. There has been considerable interest in using 9–14%Cr ODS steels in nuclear applications, including fuel cladding for fast reactors and fusion systems [36–38]. However, prior work had shown that ODS Fe–13Cr had poor oxidation resistance in laboratory air above 900 °C [39]. Rather than evaluating each of the candidate ODS Fe–Cr alloys, the model alloy results suggest that none of the current ODS Fe–Cr alloys with only 9–14%Cr will be protective at 1200 °C in this environment. This conclusion was verified by the results on the ODM401 alloy with 14%Cr, Fig. 9.

There are always difficulties in recreating complex environments in the laboratory. As noted above, the choice of reaction tube (SiC for the high pressure tests above 1000 °C, quartz for the TGA) will affect the partial pressure of reactant species, i.e. $Si(OH)_4$, as both the specimen and reaction tube will react. However, it was not possible to change the reaction tubes on these systems and even alumina reaction tubes will begin to react and form $Al(OH)_3$ at higher steam temperatures. For the CVD SiC oxidation, the presence of additional $Si(OH)_4$ vapor from the reaction tube along with the relatively low gas velocities in both the high pressure and TGA systems limited the amount of volatilization in these experiments. Therefore, the reaction layers observed were thicker with less material recession than would be observed with a higher gas velocity [21]. Nevertheless, for the relatively short times of interest for this application, SiC likely has sufficient oxidation resistance. For all Si-based ceramics, concerns about the oxidation resistance in the presence of water vapor are more important for long-term applications [7,11,21]. It is worth noting that the parabolic fits for the TGA data were better for the metals and less relevant for CVD SiC, which could have been fit to a linear rate. A parabolic rate was used only to assist in the comparison with the other materials in Fig. 5a.

Based on this high temperature oxidation data, FeCrAl-type alloys and high-Cr Fe–Cr appear the most promising materials for further consideration in this application and SiC-based ceramics also have significantly lower reaction rates. Several FeCrNi alloys, like 310SS, showed protective behavior at 1200 °C in steam, Fig. 7a.

However, Ni is not generally desirable for fuel claddings because of its high thermal neutron absorption cross-section (almost twice that of Fe) and formation of radioactive Co (through $^{58}N(n,p)^{58}Co$ reaction with fast neutrons) in the core [3]. The Ni content can explain the relatively poor oxidation performance of type 304L with its lower Ni content and the superior performance of the high Ni austenitics such as HR120 and type 310 stainless steel, Table 1.

The alumina-forming FeCrAl alloys are very resistant to these environments and form protective alumina scales up to 1475 °C [40], close to the liquidus temperature of ~1500 °C. To counter the neutronics penalty compared to Zr alloys [8,9], thinner FeCrAl cladding walls may be possible. To illustrate its protective behavior even with thin sections, a ~130 μm thick PM2000 foil specimen also was exposed at 1200 °C and formed a similar thin protective oxide to that on the 1.5 mm thick specimen shown in Fig. 9f. One surprising result was the poor oxidation resistance of lean FeCrAl alloys in steam or Ar–H_2O at 1200 °C, Figs. 5b and 7a. These alloys were unable to form alumina and were largely consumed during this exposure. This emphasizes the effect of total composition on oxidation resistance and the need for further work to define sufficient Cr and Al levels for protective behavior in this application.

For any of these candidates, substantially more work is needed to study the corrosion resistance and mechanical behavior in pressurized and boiling water at ~320 °C and the effects of irradiation on these alloys (especially Cr-rich α' formation under irradiation) because these alloys have not been previously considered for fuel cladding applications.

Future high temperature screening work will focus on 1 bar steam at 1200 °C and higher temperatures as the higher pressure and addition of H_2 did not appear to have a strong effect on the most oxidation resistant alloys. Currently, model Fe–Cr–Mn–Si−Y and Fe–Cr–Al ± Y alloys are being evaluated to determine the critical compositions needed for steam oxidation resistance [40]. For the Fe–Cr alloys, the binary model alloys provide important starting information. However, as was observed with the Fe–20Cr–20Ni alloy, additions of elements such as Mn, Si and La can substantially improve oxidation resistance (Figs. 7a and 8d) in the presence of water vapor and reduce the critical amount of Cr needed for oxidation resistance [30]. The ODS Fe–14Cr alloy performed better than the Fe–15Cr model alloy. For FeCrAl alloys, lowering the Al and Cr contents from the typical 20Cr–5Al composition could result in an alloy more suitable for thin walled tubing with better mechanical properties and weldability.

5. Summary

Initial experiments were conducted at 800–1350 °C in 1–20 bar steam and H_2–H_2O environments to determine relevant experimental conditions and promising candidates for future study as more accident tolerant fuel claddings to replace Zr alloys in light water reactors. Materials that can form protective alumina (such as FeCrAl) and silica (e.g. CVD SiC) showed minimal attack up to 1350 °C in 3.4 bar steam. A range of commercial and model alloys was used to illustrate the effects of alloy composition on steam oxidation resistance for this application. Conventional ~18Cr–10Ni stainless steels do not have sufficient oxidation resistance for the highest temperatures under consideration. Increasing the Cr and/or Ni contents increased the steam oxidation resistance at 1200 °C, as in type 310 stainless steel (25Cr–20Ni). However, high Ni contents are not desirable for this application. High Cr ($\geqslant$25%) ferritic steels appear to be promising candidates but chromia-forming alloys were generally not as resistant as the alumina-forming alloys or SiC at higher temperatures. Higher pressures and H_2 additions appeared to have minimal effect on the oxidation resistance of the most protective materials. Higher steam partial pressures increased the maximum metal loss at 1200 °C for 317L stainless steel.

Acknowledgments

The experimental work was conducted by M. Howell, M. Stephens, T. Lowe, H. Longmire, J. Mayotte and T. Jordan. Y. Yamamoto and S.J. Pawel provided useful comments on the manuscript. This research was funded by the U.S. Department of Energy's Office of Nuclear Energy, Advanced Fuel Campaign of the Fuel Cycle R&D program.

References

[1] R. Gauntt, et al., Sandia National Laboratory Report, SAND2012-6173, Albuquerque, NM, 2012.
[2] D. Powers, R. Meyer, US NRC Report, NUREG-0630, 1980.
[3] K.A. Terrani et al., J. Nucl. Mater. (2013) (submitted for publication).
[4] P. Yvon, F. Carré, J. Nucl. Mater. 385 (2009) 217.
[5] L. Hallstadius, S. Johnson, E. Lahoda, Prog. Nucl. Energy 57 (2012) 71.
[6] Y. Katoh, L.L. Snead, I. Szlufarska, W.J. Weber, Curr. Opin. Solid State Mater. Sci. 16 (2012) 143.
[7] E.J. Opila, Mater. Sci. Forum 461–464 (2004) 765.
[8] J.E. Rivera, J.E. Meyer, MIT-EL Report #80-021, Cambridge, MA, 1980.
[9] A. Strasser, et al., EPRI Report # NP-2642, Palo Alto, CA, 1982.
[10] T. Cheng, J.R. Keiser, M.P. Brady, K.A. Terrani, B.A. Pint, J. Nucl. Mater. 427 (2012) 396–400.
[11] K.L. More, P.F. Tortorelli, M.K. Ferber, L.R. Walker, J.R. Keiser, N. Miriyala, W.D. Brentnall, J.R. Price, J. Eng. Gas Turbines Power 122 (2000) 212.
[12] B.A. Pint, ORNL Report TM-2012/254, Oak Ridge, TN, July 2012.
[13] V.F. Urbanic, T.R. Heidrick, J. Nucl. Mater. 75 (1978) 251.
[14] R.E. Pawel, J.V. Cathcart, R.A. McKee, J. Electrochem. Soc. 126 (1979) 1105.
[15] M. Moalem, D.R. Olander, J. Nucl. Mater. 182 (1991) 170.
[16] R. Peraldi, B.A. Pint, Oxid. Met. 61 (2004) 463.
[17] T. Ishida, Y. Harayama, S. Yaguchi, J. Nucl. Mater. 140 (1986) 74.
[18] B. Jönsson, R. Berglund, J. Magnusson, P. Henning, M. Hättestrand, Mater. Sci. Forum 461–464 (2004) 455.
[19] B.A. Pint, Oxid. Met. 45 (1996) 1.
[20] B.A. Pint, J. Am. Ceram. Soc. 86 (2003) 686.
[21] E.J. Opila, R.E. Hann Jr., J. Am. Ceram. Soc. 80 (1997) 197.
[22] B. Pieraggi, Oxid. Met. 27 (1987) 177.
[23] C.S. Tedmon, J. Electrochem. Soc. 113 (1966) 766.
[24] D.J. Young, B.A. Pint, Oxid. Met. 66 (2006) 137.
[25] P.T. Moseley, K.R. Hyde, B.A. Bellamy, G. Tappin, Corr. Sci. 24 (1984) 547.
[26] G.C. Rybicki, J.L. Smialek, Oxid. Met. 31 (1989) 275.
[27] H. Buscail, S. Heinze, P. Dufour, J.P. Larpin, Oxid. Met. 47 (1997) 445.
[28] J. Engkvist, S. Canovic, K. Hellström, A. Järdnäs, J.-E. Svensson, L.-G. Johansson, M. Olsson, M. Halvarsson, Oxid. Met. 73 (2010) 233.
[29] R.C. Lobb, J.A. Sasse, H.E. Evans, Mater. Sci. Technol. 5 (1989) 828.
[30] B.A. Pint, R. Peraldi, P.J. Maziasz, Mater. Sci. Forum 461–464 (2004) 815.
[31] J. Quadakkers, L. Singheiser, Mater. Sci. Forum 369–72 (2001) 77.
[32] W. Assassa, P. Guiraldenq, Metal Sci. (1978) 123.
[33] J.H. Lee, R. Kasada, A. Kimura, T. Okuda, M. Inoue, S. Ukai, S. Ohnuki, T. Fujisawa, F. Abe, J. Nucl. Mater. 417 (2011) 1225.
[34] H. Hadraba, B. Kazimierzak, L. Stratil, I. Dlouhy, J. Nucl. Mater. 417 (2011) 241.
[35] I.G. Wright, R.B. Dooley, Int. Mater. Rev. 55 (3) (2010) 129.
[36] S. Ukai, M. Harada, H. Okada, M. Inoue, S. Nomura, S. Shikakura, K. Asabe, T. Nishida, M. Fujiwara, J. Nucl. Mater. 204 (1993) 65–73.
[37] G.R. Romanowski, L.L. Snead, R.L. Klueh, D.T. Hoelzer, J. Nucl. Mater. 283–287 (2000) 642.
[38] R.L. Klueh, J. Nucl. Mater. 341 (2005) 103.
[39] B.A. Pint, I.G. Wright, Oxid. Met. 63 (2005) 193.
[40] B.A. Pint, Unpublished data, 2013.